Available online at www.sciencedirect.com
ScienceDirect
Optics Communications 275 (2007) 223–229
OPTICS COMMUNICATIONS
www.elsevier.com/locate/optcom

Width-tunable pulse generation using four-wave mixing in bismuth based highly nonlinear fiber

Khurram Karim Qureshi [a,b,*], Shao-Hao Wang [a,b], P.K.A. Wai [a,b], Hwa Yaw Tam [a,c], Chao Lu [a,b], N. Sugimoto [d]

[a] Photonics Research Center, The Hong Kong Polytechnic University, Hung Hom, Kowloon, Hong Kong SAR, China
[b] Department of Electronic and Information Engineering, The Hong Kong Polytechnic University, Hung Hom, Kowloon, Hong Kong SAR, China
[c] Department of Electrical Engineering, The Hong Kong Polytechnic University, Hung Hom, Kowloon, Hong Kong SAR, China
[d] Asahi Glass Co. Ltd., 1150 Hazawa-cho, Yokohama 221-8755, Japan

Received 15 August 2006; received in revised form 28 February 2007; accepted 5 March 2007

Abstract

This communication reports a simple configuration for the implementation of a compact and all-fiber based width-tunable pulse generator using four-wave mixing (FWM) effect in only 1.9-m of bismuth oxide based highly nonlinear fiber (Bi-HNLF). The width- tunable pulses are generated at repetition rates of 5 and 10 GHz. In the performed experiment, the pulsewidth of a 5 GHz repetition rate pulse train is tuned from 83 to 23 ps whereas the pulsewidth of a 10 GHz repetition rate pulse train is continuously tuned from 32 to 18 ps. An analytical model is presented for width-tunable pulse generation and the results agree well with the experimental findings. The effects of pump source timing jitter and intensity fluctuation on pulse generation are discussed.

PACS: 42.65.Ky; 42.65.Re; 42.81.Wg

Keywords: Nonlinear optics; Four-wave-mixing (FWM); Optical fiber devices

1. Introduction

Optical sources capable of generating pulses with tunable pulsewidth are useful to applications such as long haul transmission systems, optical sampling and all-optical signal processing [1,2]. For example; pulsewidth of a return-to-zero (RZ) format can be optimized to provide the best immunity against fiber transmission impairments. Recently, various schemes demonstrating width-tunable RZ pulse generation using different techniques have been proposed [1–6]. Chernikov et al. [1], achieved width-tunable pulse generation by changing the biasing and driving conditions of an electro-absorption modulator (EAM) and compressed the generated pulse using a chirped grating or an adiabatic pulse compressor. The scheme offers a limited extinction ratio and the system performance is affected by the dispersion ripple of the pulse compressor. By applying spectral line-by-line pulse shaping technique in a mode-locked laser, Jiang et al. [3] reported tunable RZ pulse generation at 10 GHz. Although a wide tuning range was demonstrated, a large insertion loss of 15 dB was introduced by the grating-based pulse shaper [4]. There has recently been renewed interest in fiber based configurations for width-tunable pulse generation [6,7,11,12]. By employing different kinds of fibers as a nonlinear media, width-tunable pulse generation has been achieved by utilizing FWM effect. Yu et al. [6] proposed using 1 km of highly nonlinear fiber, whereas Zhang et al. [7] proposed using

* Corresponding author. Address: Department of Electronic and Information Engineering, The Hong Kong Polytechnic University, Hung Hom, Kowloon, Hong Kong SAR, China. Tel.: +86 852 27664094; fax: +86 852 23628439.
E-mail addresses: kqureshi94@gmail.com, enkkq@eie.polyu.edu.hk (K.K. Qureshi).

0030-4018/$ - see front matter © 2007 Elsevier B.V. All rights reserved.
doi:10.1016/j.optcom.2007.03.013

20 m of photonic crystal fiber (PCF). In these two configurations, by tuning the relative delay between the two pump pulse trains, the pulsewidth of pulse train generated by FWM effect can be continuously tuned. To further improve system performance using this scheme, short fiber length is preferred in order to reduce insertion loss and the effect of chromatic dispersion.

In recent years, the optical fiber fabrication technology based on bismuth oxide material has advanced significantly and has resulted in the production of highly nonlinear Bi_2O_3 fiber [8]. This type of fiber acts as an effective nonlinear media for realizing the all-optical devices. One of the most striking features of this fiber is its ultra high nonlinear coefficient, which is 100 times larger than that of silica-based highly nonlinear fiber (HNLF) [9]. Therefore, it can offer strong nonlinear effect in a relatively short length (~1 m) of fiber. In addition, Bi-HNLF has a relatively high stimulated Brillouin scattering (SBS) threshold [10]. Hence, SBS suppression schemes are not required when using high pump powers. We recently reported [11] width-tunable pulse generation, where the pulsewidths are tuned over a wide tuning range for 5 and 10 GHz repetition rate systems respectively. In a similar reported work, 10 nm tuning range of the generated pulse is achieved [12]. Here we report width-tunable pulse generation at a repetition rate of 5 and 10 GHz as well as theoretically study the pulse generation based on FWM effect in only 1.9-m of Bi-HNLF. A good agreement between the experimental and prediction results is observed. The effects of pump source timing jitters and intensity fluctuations prove to be the main limiting factors for the generation of ultra-short pulses.

In Section 2, the experimental results regarding width-tunable pulse generation at 5 and 10 GHz, respectively are reported. Section 3 reports the theoretical works based on experimental results and finally Section 4 concludes this communication.

2. Experimental results

Fig. 1 shows the schematic of the experimental setup to demonstrate the proposed all-optical width-tunable pulse generation using Bi-HNLF. The pump signals are generated by externally modulating a tunable laser (TL-1) at 1552.84 nm and another tunable laser (TL-2) at 1553.64 nm with electro-optic Lithium Niobate ($LiNbO_3$) modulators driven by a 5 or 10 GHz RF clock signal generated by pulse pattern generator (PPG). The electro-optic modulator has a large extinction ratio of ~15 dB at the selected operating point. The wavelength separation between two pump signals is chosen to be 0.8 nm. The relative time delay between the two pump pulses train can be continuously tuned using the internal electrical delay line of the PPG. A polarization controller (PC3) placed after the modulator (MOD-1) is used to optimize the conversion efficiency of the FWM process inside the Bi-HNLF by aligning the states-of-polarization of the two pulse trains. The two pulse trains are then combined using a 3-dB coupler and are amplified to a peak power of ~25 dBm by employing an erbium doped fiber amplifier (EDFA) with a maximum saturation output power of 27 dBm. The combined signals are then launched into 1.9-m long Bi-HNLF.

If direct fusion-splicing of the Bi-HNLF to SMF28 is done, the splicing loss will be very large because of large mode field diameter (MFD) mismatch (Bi-HNLF:2.1 μm, SMF28:10.4 μm). Therefore, ultra high NA SiO_2 fiber (UHNA4, Nufern), whose MFD is 4.0 μm is used as intermediary fiber. These fibers are fusion-spliced by arc discharge using a conventional fusion splicing machine. The total loss at the input side of the Bi-HNLF, which includes the splice loss between the SMF28 and UHNA4, the splice loss between the UHNA4 and the Bi-HNLF, and the propagation losses in the SMF28 and the UHNA4, is 1.1 dB. The total loss at the output side of the Bi-HNLF is 2.6 dB. The propagation loss of the Bi-HNLF is 2.0 dB/m at 1550 nm. The total loss of the Bi-HNLF is therefore 7.5 dB. The refractive index of the core and cladding glass are 2.22 and 2.13, respectively. Thus, the numerical aperture of this fiber is 0.64. The group velocity dispersion (GVD) and the nonlinear co-efficient of the Bi-HNLF at 1550 nm are −280 ps/nm/km and 1000/W/km, respectively. Although the Bi-HNLF has a large normal GVD coefficient, which is mainly due to the material dispersion of the high refractive index glass, the walk-off effect is not significant because of the short fiber length.

Fig. 2 shows the spectra before and after Bi-HNLF at 10 GHz clock rate. We observed a conversion efficiency of ~−16 dB for 10 GHz and ~−18 dB for 5 GHz clock

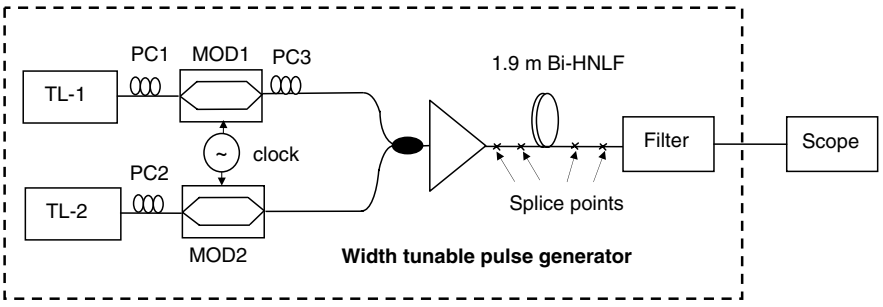

Fig. 1. Experimental setup of the width-tunable pulse generator.

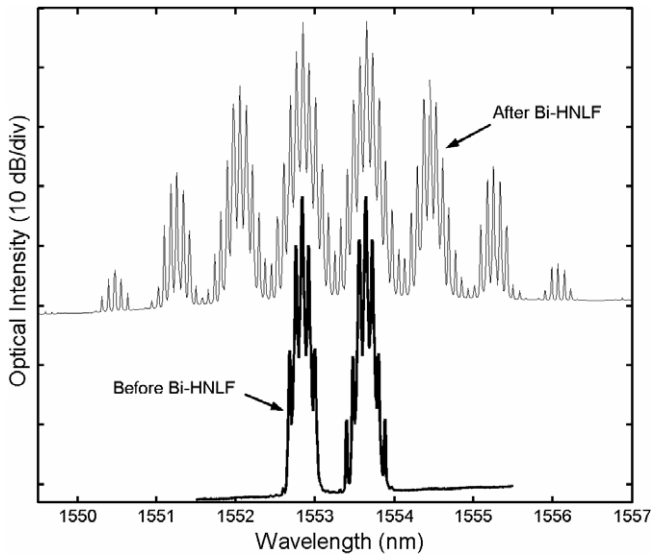

Fig. 2. Spectra at the input and output of Bi-HNLF without delay between the two pump pulses at 10 GHz repetition rate.

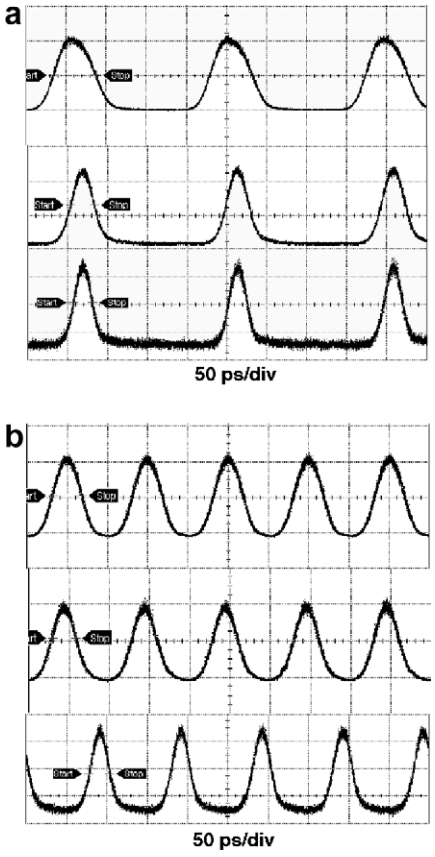

Fig. 3. (a) Temporal profiles for width-tunable pulse generation at different instances of relative pump delay at 5 GHz repetition rate. (b) Temporal profiles for width-tunable pulse generation at different instances of relative pump delay at 10 GHz repetition rate.

pulses respectively. A thin film filter with a 3-dB bandwidth of 0.6 nm and centered at 1554.44 nm is used to filter out the idler signal which contains the newly generated pulse train. The measured temporal profiles of generated pulses with different pulsewidths at repetition rates of respectively 5 and 10 GHz are shown in Figs. 3a and b. The experimental results show that the pulses are tunable from 83 to 23 ps at 5 GHz and from 32 to 18 ps at 10 GHz respectively.

3. Theory

In this section, the properties of the tunable pulsewidth pulse generator are investigated based on a simple model and using the measured data obtained from the performed experiments.

3.1. Model

Since the effect of chromatic dispersion is relatively weak compared to the nonlinear effect in this piece of Bi-HNLF, the evolution of the optical field is governed by

$$\mathrm{i}\frac{\mathrm{d}q}{\mathrm{d}z} + \gamma|q|^2 q = -\mathrm{i}\frac{\alpha}{2}q \tag{1}$$

where $q(z)$ is the slowly varying amplitude of the pulse envelope, z is length of the fiber traversed, γ is the nonlinear coefficient, and α is the attenuation coefficient. Eq. (1) only includes the nonlinear phase modulation and the attenuation effect. We assume that there is no phase mismatch between the two pump pulses. The solution of Eq. (1) is given by

$$q(z) = q(0)\exp\left\{-\frac{\alpha}{2}z + \frac{\mathrm{i}\gamma}{\alpha}|q(0)|^2[1-\exp(-\alpha z)]\right\} \tag{2}$$

The experiment can be analysed by using two pump signals with different carrier frequencies as initial condition in Eq. (2). Different frequency components, such as pumps and idlers, are selected using an ideal filter. By applying an inverse Fourier transform on these components, the relative pulse shapes of these frequency components are measured. The fiber attenuation is chosen to be 2.0 dB/m with a nonlinear coefficient of $\gamma = 1000/\mathrm{W/km}$. For simplicity, we consider the two input pulses to be identical with each pulse having a peak power of 0.4 W.

During our investigation, we found that the shape of the initial input pulse plays a key role in the evaluation of results. Since FWM is an intensity sensitive nonlinear process, the fitting of the input pulses peak shape become important. The return-to-zero (RZ) format output of the amplitude-modulated Mach-Zehnder modulator has a raised-cosine (RC) profile. However, when compared with the standard RC pulse, the experimentally observed pulse shapes at 5 GHz and 10 GHz have shorter rise times [6]. Therefore, we defined a combined RZ pulse, formed by rise/fall time of RC function with a flat pulse top. This RZ pulse was used to fit the measured pulse shape and was decided by choosing several parameters, such as pulsewidth, rise/fall time, input peak power and extinction ratio. In order to obtain a combined RZ pulse having the best fitting of the waveform data, we calculated the least square

error between the measured waveform and combined RZ pulse. Since accurate fitting at the pulse top is important in this case, weighting was added at the upper parts of pulse rising edge. Table 1 lists two groups of parameters based on two sets of data obtained from the two different modulators. In each group, two values of total least square errors are listed. They represent respectively, the combined RZ pulse obtained by using pulsewidth and rise time from the oscilloscope and the combined RZ pulse with modified values of rise time. In each group, the combined RZ pulse using the modified values of rise time produce smaller error than those using parameters obtained from the oscilloscope. In other words, by using modified parameters one can achieve a better fitting of the upper parts of input pulse. The shape of the input pulse at 10 GHz was obtained experimentally and curve fitting was applied as depicted in Fig. 4a to use it as an initial condition for the subsequent simulations. The input combined RZ pulse used for this simulation has a FWHM of 44 ps with a rise time of 26 ps which gives the minimum least square error. The output pulse shapes, when the delay between the input pump pulses is 0, 10 and 40 ps are shown respectively in Fig. 4b–d. The corresponding experimental output pulses are shown in Fig. 3b. The relationship between output idler pulsewidth versus input pump pulses delay at 5 GHz (triangles) and 10 GHz (squares) is shown in Fig. 5. The prediction results are obtained using the modified rise time of the input pulse. A good agreement is observed between the simulation results and the experimental findings.

3.2. Effect of initial pulse shape parameters on the evaluation of results

For better understanding the features of the proposed width-tunable pulse generator, the evaluation results are shown in Fig. 6. The combined RZ pulses with a fixed FWHM of 45 ps at a repetition rate of 10 GHz are used as input pulses. As depicted in Fig. 6a, for a fixed initial extinction ratio of 20 dB and input peak power of 0.4 W, steeper rise time can maximize the tuning range of the generated pulse. It is worth noting that the slope of the trace is also steeper for shorter rise time. In Fig. 6b, we fixed the rise time and extinction ratio respectively at 25 ps and 20 dB, while changing the input peak power of the two pulses. Strong nonlinear effects are introduced due to high pulse intensity in the Bi-HNLF. The increase in input

Table 1
Experimental and modified parameters

		FWHM (ps)	Rise time (ps)	Total least square error
Group one (modulator one)	Combined RZ	42.1	24.3	0.0429
	Combined RZ (modified rise time)	44	26	0.0386
Group two (modulator two)	Combined RZ	44	19.9	0.0838
	Combined RZ (modified rise time)	44	26	0.0348

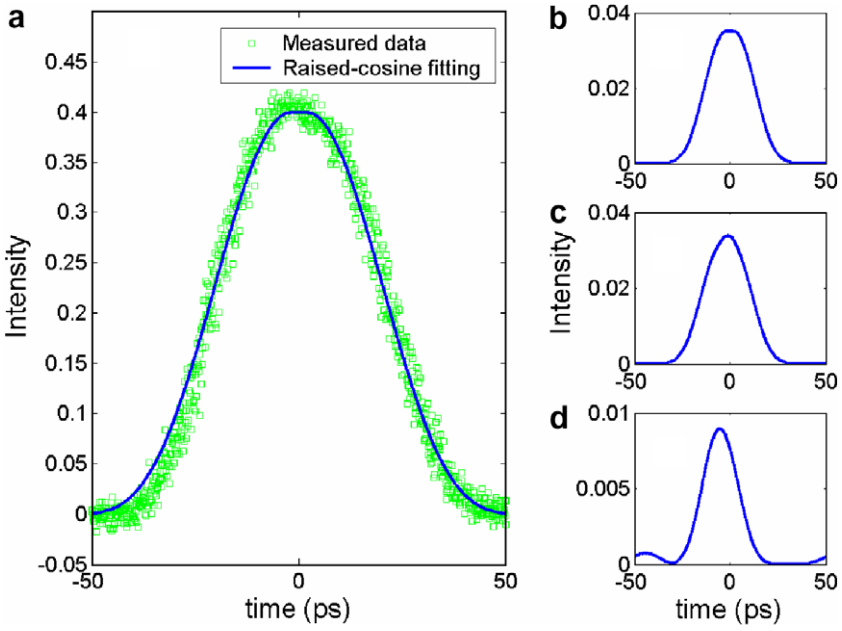

Fig. 4. (a) Measured and predicted input. (b–d) Predicted output pulse shapes at 10 GHz repetition rate. (note: outputs are obtained when the delay between the input pump pulses are repectively; 0, 10 and 40 ps).

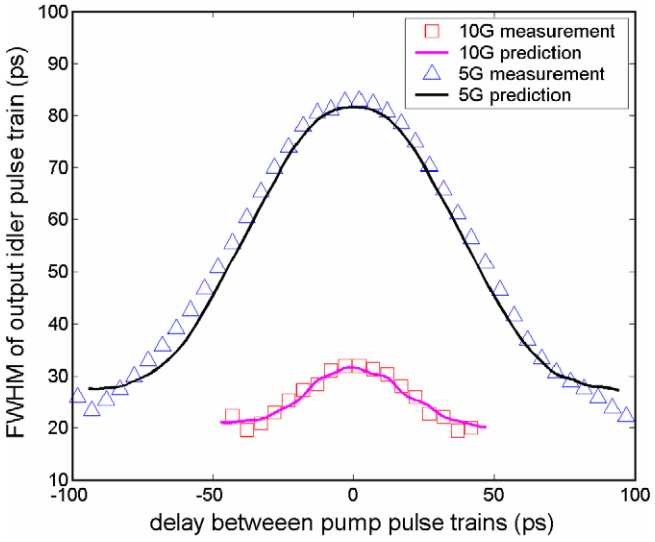

Fig. 5. Measured and predicted FWHM of generated pulses versus pump delay at 5 and 10 GHz repetition rates respectively.

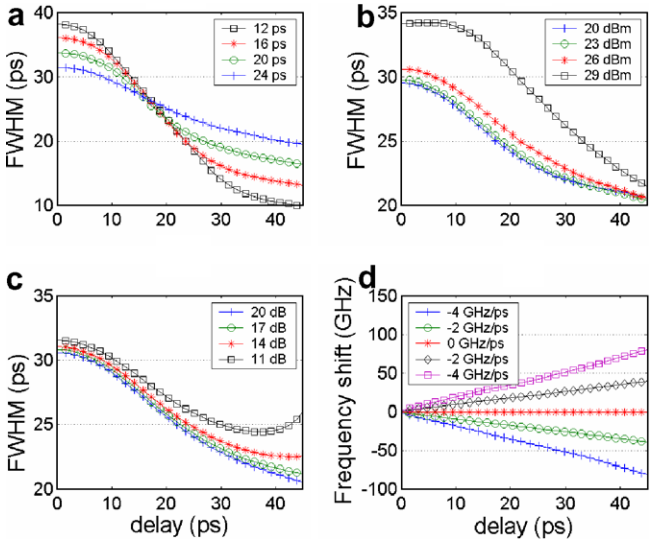

Fig. 6. Relationship between output idler pulsewidth and relative pump delay for different (a) rise time (b) input power (c) input pulse extinction ratio and (d) relationship between frequency shift and relative pump delay for different initial chirp.

power will not cause dramatic change in the trace of idler pulsewidth versus pump delay, until it reaches a threshold, which is at around an input peak power of 28 dBm per pulse (nonlinear length <1.9 m). Beyond this threshold, the spectrum of both idler and pump pulses will tend to broaden due to nonlinear phase modulation. Fig. 6c shows the effects of different extinction ratios of the input pump pulses. Due to low extinction ratio, the pedestals of input pulses introduce extra FWM effects and hence reduce the tuning range of the generated pulse. During this analysis, the rise time and peak power are kept fixed at 25 ps and 20 dBm, respectively. The effect of initial chirp on the generated pulse is also investigated and is shown in Fig. 6d. The electro-optic $LiNbO_3$ modulator used for the experiment exhibits zero chirp and does not cause any obvious frequency shift of the idler signal, whereas using a mode-locked laser output as a pump source introduces strong initial chirp and can cause extra shift in the central frequency of the idler signal. This effect may also lead to the generation of small peaks within the idler pulse. From experiments we also observed that each input pump pulse experienced a maximum timing jitter of ~300 fs.

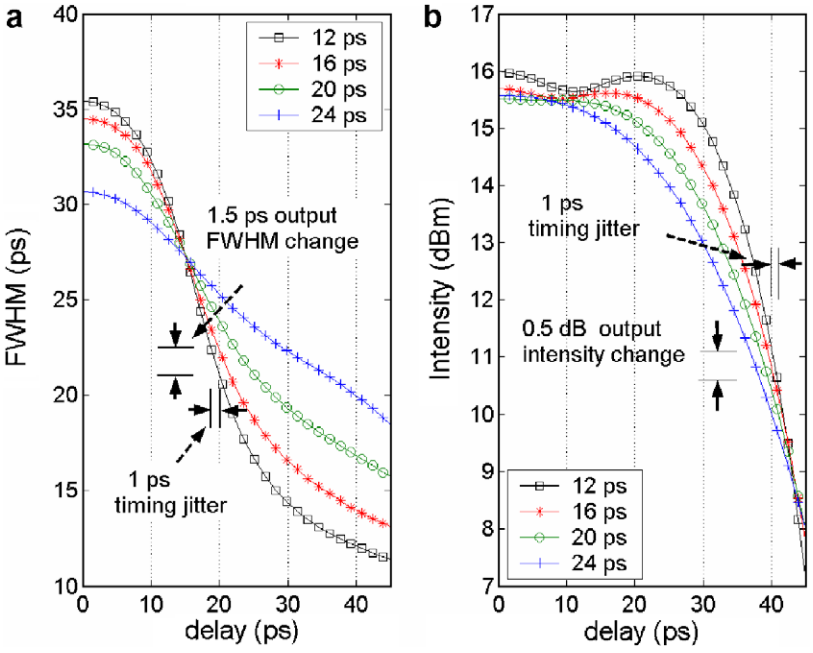

Fig. 7. (a) FWHM of generated pulses at 10 GHz versus relative pump delay for different rise time of input pulses and (b) intensity of the generated pulses versus relative pump delay.

3.3. Width-tunable pulse generation at 40 GHz

Based on the above model, a series of studies are carried out to further understand the properties of the proposed width-tunable pulse generator. The timing jitters of the width-tunable pulse generator are first analyzed. The input pump pulses timing jitters, which mainly originate from the fluctuation of electrical triggers, are the major sources of output pulse timing jitter. Fig. 7 depicts the simulation results for the relationship between the FWHM of the generated pulse versus delay between the input pump pulses at a repetition rate of 10 GHz. The results are obtained using inputs consisting of combined RZ pump pulses with fixed pulsewidths but different rise times. Short pulses of ~12 ps are generated when the input pump pulses have steeper rise time. For clarity, the trace of idler pulsewidth versus pump delay in Fig. 7 can be divided into three sections, corresponding to pump delay of 0–10, 10–25 and >25 ps, respectively. The simulations are carried out by assuming a timing jitter of 1 ps between the two input pump pulses. When the delay between the two pumps is small, the timing jitters do not have a significant effect on the output pulsewidth and peak intensity. However, for the delay from 10–25 ps, a pump delay jitter of 1 ps, may produce 1.5 ps change in the FWHM of the output pulse as depicted in Fig. 7a. When the delay between two pulses is further increased (>25 ps), 1 ps pump delay jitter may produce 0.5 dB intensity fluctuation of the output pulse as shown in Fig. 7b. From the above analysis, we can conclude that while using combined RZ pulse trains as the initial pump pulses of the width-tunable pulse generator, the stability of its output pulsewidth degrades if the pump timing jitters are large. In addition, for systems requiring relatively longer fiber, pulse walk-off effect can also introduce such degradation.

Figs. 8 and 9 show the simulation results regarding width-tunable pulse generation at 40 GHz. For simplicity, the peak power of input pulse train is chosen to be 0.4 W, the fiber length is 1.9-m, the fiber attenuation to be 2.0 dB/m and the nonlinear coefficient $\gamma = 1000/\mathrm{W/km}$. When a combined RZ pulse with a fixed pulsewidth of 12 ps at a repetition rate of 40 GHz is used as an input signal, the trace of pulsewidth versus pump delay and idler peak intensity versus pump delay at different rise times show similar trend as that of a 10 GHz system. For input pump pulses having relatively shorter rise times, the idler shows large fluctuations in the pulse intensity and pulsewidth. However, when the rise time of input pulse is 6 ps, the prediction result shows a linear relationship between the pulsewidth and the pump delay. This allows the idler pulsewidth to be continuously tuned from 8 to 4.5 ps. For the combined RZ pulse having a steeper rise time, the duration of flat top portion of the pulse is longer. Therefore, the resultant idler pulsewidth in this case is broader at zero delay between the two input pump pulses compared to the case when the rise time is longer (meaning shorter flat top portion). Hence the idler pulsewidth is dominated by the flat top portion of the input pulse. Fig. 9 shows the prediction results for a different initial condition. Here we assumed an un-chirped Gaussian pulse as an initial input signal. While assuming the two initial pulses to be identically Gaussian, we found that the output idler is also proportional to a Gaussian function. Therefore, once the pulsewidth of the initial Gaussian pulse is

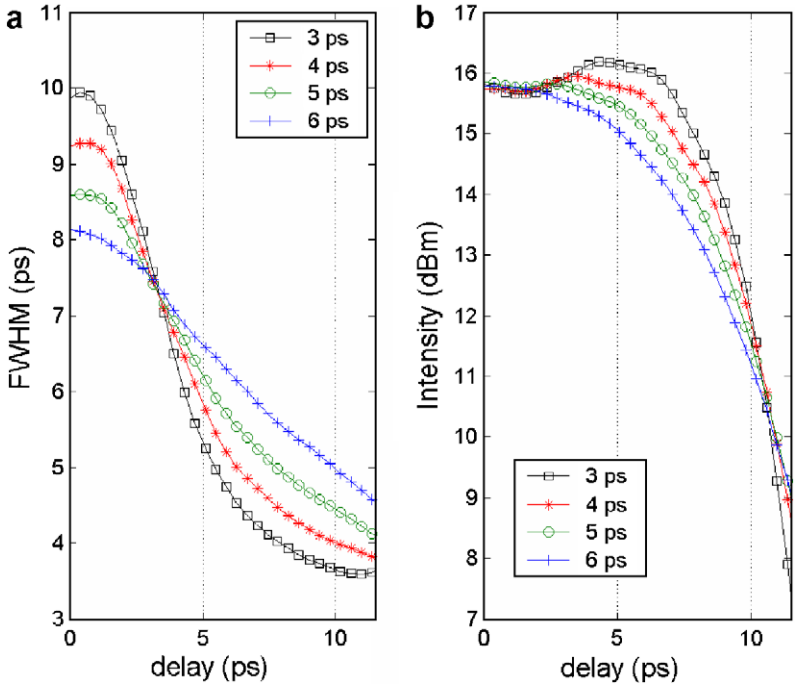

Fig. 8. (a) FWHM of generated pulses at 40 GHz versus relative pump delay and (b) intensity of generated pulse train versus relative pump delay. (note: 40 GHz combined RZ pulses with different length scale of RC rise time are used as initial condition).

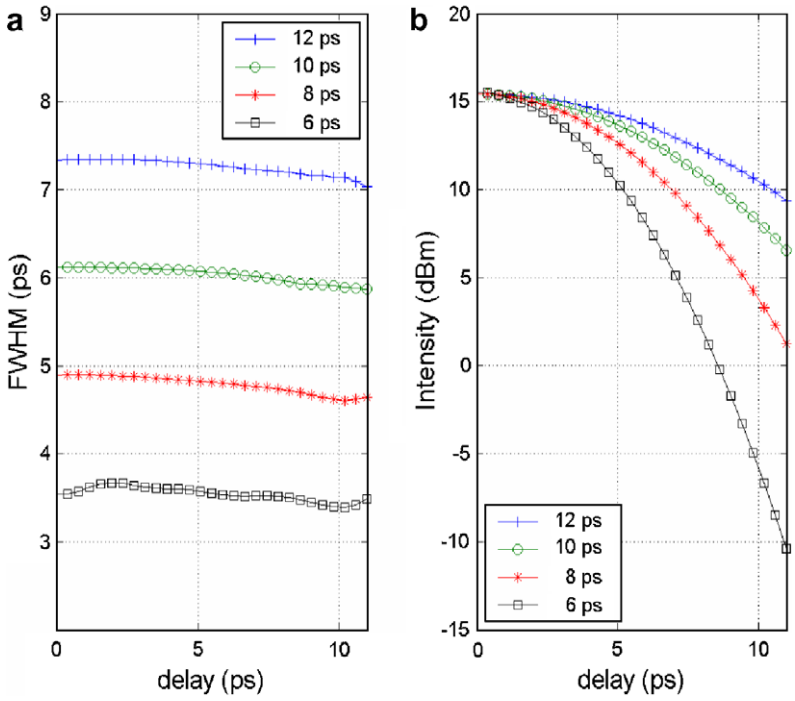

Fig. 9. (a) FWHM of generated pulses a at 40 GHz versus relative pump delay and (b) intensity of generated pulse train versus relative pump delay. (note: 40 GHz un-chirped Gaussian pulses with different input pulsewidth are used as initial condtion).

fixed, the pulsewidth of the output idler is also fixed. When the delay is introduced between the two Gaussian input pulses, the output idler pulsewidth does not change and retains its Gaussian shape. From these results, we can conclude that the pulsewidth of the idler does not vary significantly with the pump delay. The comparison also reveals that at 40 GHz repetition rate, the shape of the input RZ pulse plays an important role in deciding the tuning range of the width-tunable pulse generator.

4. Conclusion

We have experimentally demonstrated a width-tunable pulse generator using 1.9-m of Bi-HNLF. A conversion efficiency of larger than −16 dB was obtained. A simple analytical model is developed and its results agree well with the experimental findings. The output pulse train of width-tunable pulse generator is sensitive to the shape of the input pulse. The effect of pump source timing jitter proves to be an important factor in determining the quality of this width-tunable pulse source.

Acknowledgement

This research is supported by grant from the Hong Kong Polytechnic University (Project Number G-U155).

References

[1] S.V. Chernikov, M.J. Guy, J.R. Taylor, D.G. Moodie, R. Kayhyap, Opt. Lett. 20 (1995) 2399.
[2] L.S. Yan, S.M.R.M. Nezam, A.B. Sahin, J.E. McGeehan, T. Luo, Q. Yu, A.E. Willner, J. Lightwave Technol. 23 (2005) 1063.
[3] Z. Jiang, D.E. Leaird, A.M. Weiner, Photon. Technol. Lett. 17 (2005) 2733.
[4] Z. Jiang, D.E. Leaird, A.M. Weiner, Opt. Lett. 17 (30) (2005) 1557.
[5] M. Matsuura, N. Kishi, T. Miki, IEEE Photon. Technol. Lett. 17 (4) (2005) 902.
[6] C. Yu, L.S. Yan, T. Luo, Y. Wang, Z. Pan, A.E. Willner, IEEE Photon. Technol. Lett. 17 (2005) 636.
[7] A. Zhang, H. Liu, M.S. Demokan, H.Y. Tam, IEEE Photon. Technol. Lett. 17 (2005) 2664.
[8] J.H. Lee, T. Tanemura, T. Nagashima, T. Hasegawa, S. Ohara, N. Sugimoto, K. Kikuchi, Opt. Lett. 30 (11) (2005) 1267.
[9] N. Sugimoto, T. Nagashima, T. Hasegawa, S. Ohara, K. Taira, K. Kikuchi, Bismuth-based optical fiber with nonlinear coefficient of 1360 W^{-1} km^{-1}, in: Proceedings of the Optical Fiber Communications Conference (OFC 2004), LA, March 2004 (Postdeadline paper PDP26).
[10] J.H. Lee, T. Nagashima, K. Kikuchi, T. Nagashima, T. Hasegawa, S. Ohara, N. Sugimoto, Opt. Lett. 30 (2005) 1698.
[11] K.K. Qureshi, H.Y. Tam, W.H. Chung, P.K.A. Wai, N. Sugimoto, Generation of optical pulses with tunable pulsewidth using 1.9 m bismuth-based highly nonlinear fiber, CLEO, CMEE3, 2006.
[12] M. Fok, C. Shu, Wavelength and width-tunable optical pulses generated form four-wave mixing in a 35-cm bismuth oxide highly nonlinear optical fiber, OFC, OWI34, 2006.